Multi-objective Optimal Design of a Five-Phase Fault-Tolerant Axial Flux PM Motor

Harold SAAVEDRA[1], Jordi-Roger RIBA[2], Luís ROMERAL[1]
[1]*Universitat Politècnica de Catalunya, Electronic Engineering Department, Terrassa, 08222, Spain*
[2]*Universitat Politècnica de Catalunya, Electric Engineering Department, Igualada, 08700, Spain*
riba@ee.upc.edu

***Abstract*—Electric motors used for traction purposes in electric vehicles (EVs) must meet several requirements, including high efficiency, high power density and fault-tolerance. Among them, permanent magnet synchronous motors (PMSMs) highlight. Especially, five-phase axial flux permanent magnet (AFPM) synchronous motors are particularly suitable for in-wheel applications with enhanced fault-tolerant capabilities. This paper is devoted to optimally design an AFPM for in-wheel applications. The main geometric, electric and mechanical parameters of the designed AFPM are calculated by applying an iterative method based on a set of analytical equations, which is assisted by means of a reduced number of three-dimensional finite element method (3D-FEM) simulations to limit the computational burden. To optimally design the AFPM, a constrained multi-objective optimization process based on a genetic algorithm is applied, in which two objective functions are considered, i.e. the power density and the efficiency. Several fault-tolerance constraints are settled during the optimization process to ensure enhanced fault-tolerance in the resulting motor design. The accuracy of the best solution attained is validated by means of 3D-FEM simulations.**

***Index Terms*—Motor design, fault-tolerance, optimization, permanent magnet machines, sizing equations.**

I. INTRODUCTION

Transportation sectors are seeking for electrical actuator systems offering compactness, reduced weight, high reliability, fault-tolerance capability and simple maintenance requirements [1]. PMSMs offer interesting advantages including compactness, high efficiency, high torque density, high power factor or rugged designs. Therefore, PMSMs are being applied in high performance applications where variable speed is required, including servo drives, robotics, or the transportation sector [2]. In particular, AFPMs show smaller axial length than radial-flux permanent magnet machines [3] while offering enhanced torque and power densities for specific applications.

During the last decade an extensive research work about fault-tolerant operation of three-phase electrical motors and drives has been carried out [4-6]. Fault-tolerance can be ensured by using multiphase, and in special five-phase motor drives, with fractional-slot single-layer concentrated windings with physical, thermal, electrical, and magnetic isolation among phases [7,8]. It has been reported that five-phase machines are intrinsically more advantageous for fault-tolerant operation than three-phase machines, since in the event of a fault, by using the remaining healthy phases, these machines can offer continue operation [9,10]. Additional advantages of multiphase motor drives include reduced amplitude and increased frequency of the torque pulsations, reduction of the stator current per phase at the same phase voltage, reduction of the dc link current harmonics or higher torque per ampere for a given volume of the machine among others [7].

Electric motor manufacturers have always pursued the development of optimized motors, mainly aimed to minimize manufacturing costs and materials, while maintaining overall features and performance. The automotive sector is taking advantage of these improvements, thus enhancing fuel economy in electric and hybrid vehicles and reducing greenhouse gasses emissions. However, the optimal design of electrical machines is a complex issue, since it depends of several constrained design parameters which often are not independent and present nonlinear correlations due to the nonlinear behavior of the active materials [11]. Motor design objectives are often difficult to meet, as for example low-cost and high power density motors with high efficiency are often pursued. Therefore, the optimal design is not unique and a compromised final solution is often selected [11].

Optimization algorithms seek to find the optimal or satisfactory design from a broad set of feasible designs by iteratively analyzing an objective function. Optimization algorithms often analyze the possible values of the design variables, which must be confined within the feasible design space. To this end, the design variables are usually constrained within reasonable values to ensure the achievement of an optimal solution [12]. Optimization algorithms are classified into classical or deterministic and stochastic methods. Whereas the former ones use specific rules to move from one solution to the next one, stochastic algorithms apply probabilistic transition rules, thus usually being faster in locating the final solution [13]. Among stochastic algorithms, genetic algorithms (GA) are applied in a wide spectrum of applications, since GAs are recognized as unbiased optimization methods to sample a large space of solutions [14].

This paper deals with the optimal design of a five-phase fault-tolerant axial-flux PMSM which has to provide the tractive force of an electric scooter. As initial design constraints, it has a NN configuration and non-overlapping fractional-slot concentrated windings. For optimization purpose a multi-objective design strategy is applied, in which the variables to be optimized are the motor efficiency and power density and ten input geometric and electric parameters are considered, with their respective bounds and

This work was supported in part by the Spanish Ministry of Science and Technology under the TRA2013-46757-R research Project

Digital Object Identifier 10.4316/AECE.2015.01010

constraints. As explained, this is a challenging task, due to the large sets of possible solutions and the non-linear behavior of the electric motor. The motor is sized by applying an iterative method based on a set of analytical equations, which allow computing the two output variables from the input parameters values. Next, by applying a multi-objective genetic algorithm (MoGA) approach, the input parameters are modified to find out the Pareto front of the broad set of solutions explored, and from it the best solution attained is identified based on the maximum Euclidean distance to the origin point. To increase the accuracy of the AFPM design, a further refinement loop is applied, in which the air gap flux density of the final solution attained by means of the optimization process based on the analytical equations is substituted with the air gap flux density obtained through 3D-FEM simulations of the same motor. At the last, the final solution obtained through the applied procedure is validated by means of a 3D-FEM analysis. For this purpose, the values of four relevant parameters which define the machine performance, obtained through the proposed optimization process and the 3D-FEM model are compared. It is worth noting that this paper combines the optimal design of a five-phase AFPM by means of a hybrid system combining analytical equations and 3D-FEM simulations, which has been scarcely analyzed in the technical literature, with special focus on the design of fault-tolerant motors, being these the main novelties.

II. The Analyzed Machine

In this paper an AFPM synchronous machine is selected to be optimally designed. This kind of actuator is known to be very convenient for some specific applications such as direct drive in-wheel applications [15] due to the high power and torque densities [16]. It is worth noting that direct drive machines simplify the vehicle mechanical structure, thus the overall vehicle efficiency and weight are minimized. The studied machine has a torus geometry containing an internal stator and two outer rotor disks, which include the magnets. The rotor disks present a NN configuration, i.e. a north pole N facing another north pole N, which is placed at the other side of the stator [17]. Fig. 1 shows the AFPM dealt with in this paper.

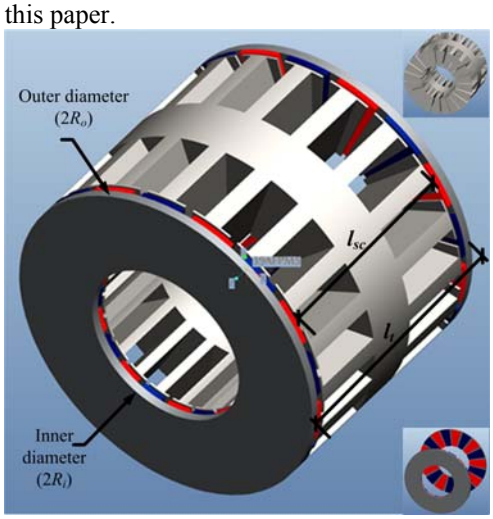

Figure 1. Dual rotor AFPM torus topology with NN configuration.

The stator core of the AFPM is made of strip wound steel and includes concentrated back-to-back connected windings, which are wounded inside the slots in the radial direction [17]. Back-to-back windings allow enhancing the overall machine efficiency, since they offer reduced end windings length, thus presenting lower copper losses [18]. In addition, both rotors contain permanent magnets with trapezoidal geometry to minimize the torque ripple [18].

Non-overlapping windings provide minimum mutual inductance between phases, thus minimizing interactions between the faulty phase and the others, so they are highly recommended in fault-tolerant machines. In addition, the design should ensure low mutual coupling among phases to limit the effect of the short circuit in one phase on other phases. The use of concentrated stator windings (i.e. windings encircling a single stator tooth, thus eliminating end-winding overlap among phase windings) offer several advantages compared to distributed windings, including a reduction of the copper volume of the end windings, which is especially significant when the axial length of motor is small, thus minimizing copper losses and improving the motor efficiency [7],[19] compared to stator windings with integer number of slots per pole and per phase. They also allow reducing the total length of the machine and manufacturing costs since concentrated windings are easier to realize. Finally, an important advantage is that compared to distributed windings, concentrated windings tend to provide higher inductance when the magnetic flux linkage is the same, which allows extending the flux-weakening region [19]. Since in this particular design the fault-tolerance is a must, a concentrated non-overlapping fractional-slot single-layer winding has been selected, as shown in Fig. 2, since it provides enough magnetic and electric insulation to avoid a major propagation of a short circuit in the event of a short circuit fault.

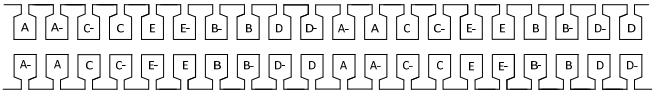

Figure 2. Layout of the fractional-slot single-layer concentrated winding structure applied in this paper.

III. Sizing Equations of the Five Phase Machine

This section develops the sizing equations to design the five-phase AFPM as described in [20],

The mechanical and electrical speeds in rad/s are, respectively,

$$\omega_m = \frac{2\pi f}{p} \tag{1}$$

$$\omega_e = p \cdot \omega_m \tag{2}$$

f and p being, respectively, the electrical frequency and the number of pole pairs.

The torque can be obtained from the output mechanical power as,

$$T_{out} = P_{out} / \omega_m \tag{3}$$

The number of slots per pole and per phase is,

$$q = Q/(2 \cdot p \cdot m) \tag{4}$$

Q being the number of slots and m the number of phases. The coil-pole fraction is defined as,

$$\alpha_{cp} = 2p / Q \tag{5}$$

The angular pole and slot pitches are as follows,

$$\theta_p = \pi / p \tag{6}$$

$$\theta_s = 2\pi / Q \tag{7}$$

The slot pitch in electrical radians is,

$$\theta_{se} = 2\pi \cdot p / Q \tag{8}$$

The inside and outside pole pitches are,

$$\tau_{pi} = R_i \theta_p \tag{9}$$

$$\tau_{po} = R_o \theta_p \tag{10}$$

R_i and R_o being, respectively, the inner and outer rotor radius. The inside and outside coil pitches are, respectively,

$$\tau_{ci} = \alpha_{cp} \tau_{pi} \tag{11}$$

$$\tau_{co} = \alpha_{cp} \tau_{po} \tag{12}$$

And the inner slot pitch is calculated as,

$$\tau_{si} = R_i \theta_s \tag{13}$$

The distribution factor required to calculate the winding factor is as follows,

$$k_d = \frac{\sin(\pi/2m)}{(Q/2pm)\sin(\pi p/Q)} \tag{14}$$

When q is a fractional number less than 1, the pitch factor k_p can be defined as the ratio between the vectorial and the arithmetic sum of the EMFs per coil side [21],

$$k_p = \sin(\pi p / Q) \tag{15}$$

In addition the skew factor is,

$$k_s = 1 - \theta_{se} / (2\pi) = 1 - p / Q \tag{16}$$

And the magnet fraction is,

$$\alpha_m = \tau_m / \tau_p = 1 - \frac{2p\tau_f}{\pi(R_o - R_i)} \tag{17}$$

where τ_m and τ_f are, respectively, the permanent magnet and spacer widths shown in Fig. 3.

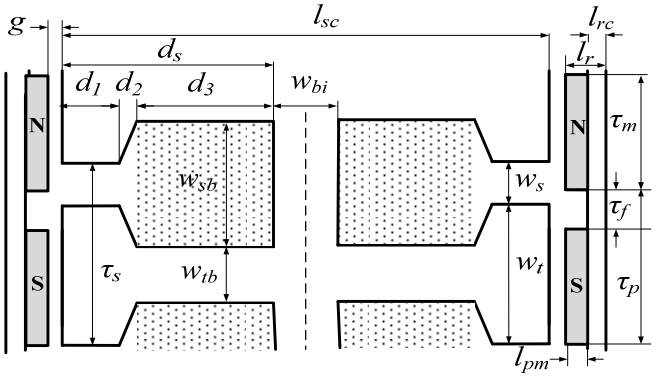

Figure 3. Sketch of the stator and rotor dimensions.

The permanent magnet leakage factor is,

$$k_{ml} = 1 + \frac{4 \cdot l_{pm} p}{\pi^2 \mu_R \alpha_m (R_o + R_i)} \ln(1 + \pi g / \tau_f) \tag{18}$$

where l_{pm} is the permanent magnet length, μ_R is the relative permeability of the magnet and g the airgap length.

The effective air gap to calculate the Carter coefficient is,

$$g_c = 2g + l_{pm} / \mu_R \tag{19}$$

And the Carter coefficient is calculated as,

$$k_c^{-1} = 1 + \frac{\omega_s}{\tau_{si}(5g_c / \omega_s + 1)} \tag{20}$$

where w_s is the slot opening, as show in Fig. 3.

The air gap area is as follows,

$$A_s = \pi(1 + \alpha_m)(R_o^2 - R_i^2)/(4p) \tag{21}$$

The average value of the air gap flux density is,

$$B_g = \frac{C_\theta}{1 + \mu_R k_c k_{ml} / P_c} B_r \tag{22}$$

B_r being the remanence of the permanent magnets and C_θ and P_c, respectively, the flux concentration factor and the permeance coefficient,

$$C_\theta = 2\alpha_m / (1 + \alpha_m), \qquad P_C = l_{pm} / (2gC_\theta) \tag{23}$$

The air gap flux is calculated as,

$$\phi_g = B_g A_g \tag{24}$$

The stator back iron width is,

$$w_{bi} = \frac{B_g \tau_{po}}{2B_{\max} k_{st}} \tag{25}$$

k_{st} being the lamination stacking factor.

The stator tooth width calculated at the inner radius is,

$$w_{tbi} = \frac{B_g \tau_{pi}}{2N_{sm} B_{\max} k_{st}} \tag{26}$$

B_{max} being the maximum allowable flux density in the stator yoke.

The slot bottom width is,

$$w_{sb} = \tau_{si} - w_{tbi} \tag{27}$$

The slot aspect ratio at the bottom width,

$$\alpha_{si} = w_{sb} / (w_{tbi} + w_{sb}) \tag{28}$$

The shoe depth split between d_1 and d_2,

$$d_1 = \alpha_{sd} w_{tbi} - d_2 \tag{29}$$

α_{sd} being the shoe depth fraction, which is defined as,

$$\alpha_{sd} = \frac{d_1 + d_2}{w_{tb}} \tag{30}$$

The number of turns per slot is,

$$n_s = \text{int}\left(\frac{E_{\max}}{2pk_d k_p k_s B_g q \omega_m (R_o^2 - R_i^2)} \right) \tag{31}$$

The peak value of the back-EMF,

$$E_{\max} = 2pk_d k_p k_s B_g q \omega_m n_s (R_o^2 - R_i^2) \tag{32}$$

The peak value of the slot current,

$$I_s = \frac{T_{out}}{2pk_d k_p k_s B_g q (R_o^2 - R_i^2)} \tag{33}$$

The peak value of the phase current is,

$$I_{ph} = I_s / (mn_s) \tag{34}$$

The conductor slot depth is obtained from the area required to fit the conductors according to the allowable current density,

$$d_3 = I_s / (k_{cp} w_{sb} J_{\max}) \tag{35}$$

Assuring rectangular slots, the slot area is,

$$A_s = w_{sb} d_3 \tag{36}$$

The conductor current density is

$$J_c = I_s / (k_{cp} A_s) \tag{37}$$

where k_{cp} is the slot fill factor, typically less than 60% (set to 50%) and A_{load} is the stator electrical loading, which can be calculated as,

$$A_{load} = 2mn_s \frac{I_{ph}}{\pi(R_o + R_i)} \tag{38}$$

According to Fig. 3, the stator tooth height is,

$$d_s = d_1 + d_2 + d_3 \tag{39}$$

AFPMs present protrusions in both the axial and radial directions, whose magnitude depends on the stator electrical loading A_{load} current density J_c, and copper fill factor k_{cp}.

The inner protrusions along the axial length can be calculated as [23],

$$W_{cui} = \sqrt{R_i^2 + \frac{A_{load}(R_i + R_o)}{k_{cp} J_c}} - R_i \quad (40)$$

The effective stack or axial length of the AFPM depends on the rotor and stator axial lengths as,

$$l_t = l_s + 2l_r + 2g \quad (41)$$

From manufacturer's experience, the effective axial length of the stator is related to the stator core axial length and the amplitude of the inner protrusions W_{cui} as,

$$l_s = l_{sc} + 1.6W_{cui} \quad (42)$$

The minimum value of the stator core axial length also may be calculated from the flux densities in the air gap B_g and in the stator core B_{sc} and the geometric ratio $\lambda = R_i/R_o$ as,

$$l_{sc,\min} = \pi B_g R_o (1+\lambda)/(2B_{sc} p) \quad (43)$$

This minimum value of $l_{sc,\min}$ is imposed to avoid a possible saturation and extra losses in the stator laminations. The new stator axial length is then computed from the total slot depth and the stator yoke width as,

$$l_{sc} = 2d_s + w_{bi} \geq l_{sc,\min} \quad (44)$$

Since the value of l_{sc} calculated in (44) must be greater or equal than that in (43) to avoid stator laminations saturation, when $l_{sc} \leq l_{sc,min}$ the value of w_{bi} must be increased to satisfy (44), so it starts a new iteration from (25). The axial length of the rotor l_r is calculated from the axial length of the rotor core l_{rc} and the length of the permanent magnets l_{pm} as,

$$l_r = l_{rc} + l_{pm} \quad (45)$$

The axial length of the rotor core l_{rc} may be expressed as,

$$l_{rc} = \pi B_g R_o (1+\lambda)/(4C_\theta B_{rc} p) \quad (46)$$

B_{rc} being the flux density in the rotor core. It is worth noting that B_{rc} is almost stationary since it is mostly due to the permanent magnets placed in the rotor discs, whereas the ac magnetic flux mainly flows through the stator core.

The peak flux density in the slots is,

$$B_{s,\max} = \mu_o I_s /(w_s) \quad (47)$$

The slot resistance is,

$$R_s = \rho n_s^2 (R_o - R_i)/(A_s k_{cp}) \quad (48)$$

And the end-turn resistance is calculates as,

$$R_e = \rho n_s^2 (\tau_{co} - \tau_{ci})/(4A_s k_{cp}) \quad (49)$$

The phase resistance is obtained from the slot and end-turn resistances as,

$$R_{ph} = 2N_{sp}(R_s + R_e) \quad (50)$$

The air gap inductance,

$$L_g = \frac{n_s^2 \mu_o \mu_R \theta_C k_d (R_o^2 - R_i^2)}{4(l_{pm} + 2\mu_R k_c g)} \quad (51)$$

The slot leakage inductance is,

$$L_s = n_s^2 (R_o - R_i)\left[\frac{\mu_o d_3}{3w_{sb}} + \frac{\mu_o d_2}{(w_s + w_{sb})/2} + \frac{\mu_o d_1}{w_s}\right] \quad (52)$$

and the end-turn inductance,

$$L_e = \frac{n_s^2 \mu_o \tau_{co}}{16} \ln\left(\frac{\tau_{co}^2}{4A_s}\right) + \frac{n_s^2 \mu_o d_1}{16} \ln\left(\frac{\tau_{ci}^2 \pi}{4A_s}\right) \quad (53)$$

Finally, the total phase inductance is,

$$L_{ph} = 2N_{sp}(L_s + L_g + L_e) \quad (54)$$

Both the slot opening w_s and the slot depth d_3 have a great impact on the leakage inductance, since when the first one lowers and/or the last one rises, the slot leakage inductance L_s in (52) increases. Under fault conditions, a high inductance limits the rate of change of the current while increasing the amount of time available to detect such a fault. However, as a high inductance increases the electric time constant, it makes the motor more difficult to drive. As a result, a tradeoff exists.

The Joule losses in the stator conductors are,

$$P_{Jl} = mR_{ph} I_{ph}^2 \quad (55)$$

The total core losses are,

$$P_{cl} = \rho_{bi} V_{st} p_{spec} \quad (56)$$

ρ_{bi} being the lamination mass density, p_{spec} the steel laminations specific loss (see Fig. 4), and V_{st} the volume of the stator steel laminations, which is calculated as,

$$V_s = 2k_{st}[\pi(R_o^2 - R_i^2)(w_{bi} + d_s) - QA_s(R_o - R_i)] \quad (57)$$

k_{st} is the stacking factor of the magnetic core.

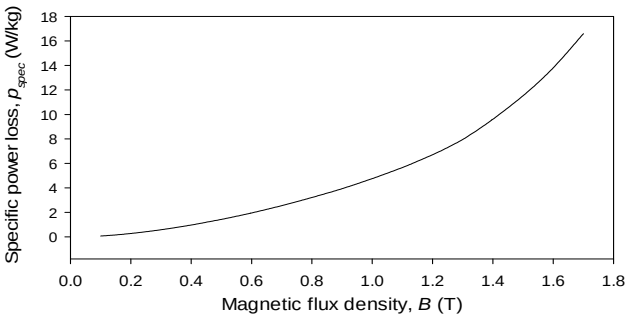

Figure 4. M330-35A steel laminations. Specific core loss versus magnetic flux density at 165 Hz.

The overall efficiency is,

$$\eta = \frac{T\omega_m}{T\omega_m + P_{Jl} + P_{cl} + P_{sl}} \quad (58)$$

where P_{sl} are the stray losses, which are mainly composed of friction, windage, and other minor components. This paper assumes P_s as 1% of the output power [22].

Finally, the power density is calculated from the mechanical output power P_{out} and the AFPM volume as,

$$P_{den} = P_{out} /(\pi R_o^2 l_t) \quad (59)$$

IV. Specifications For Maximizing Fault Tolerance

As explained, multiphase machines are well suited for fault-tolerant applications. However, to further improve fault-tolerant capability, other requirements must be fulfilled, including magnetic, electrical, physical and thermal isolation among phases [24] to minimize the possibility of phase-to-phase faults occurrence. This condition may be achieved by using non-overlapping single-layer fractional-slot concentrated windings around each tooth [7],[25] because in this configuration the phase windings are arranged in independent modules. Whereas magnetic isolation minimizes the voltages induced in adjacent phases due to a fault current in the faulty phase, physical and thermal isolation allows reducing the risk of occurrence of faults between nearby phases. Finally, to ensure electrical isolation among phases it is also highly desirable to connect each phase to a distinct single-phase

full-bridge PWM converter since each power switch has to withstand the phase voltage instead of the line voltage in star-connected systems [7].

To ensure a high level of fault-tolerance capability in the analyzed five-phase AFPM some restrictions are imposed as follows [26],

1. It is suggested to use non-overlapping fractional-slot single -layer concentrated windings. These windings tend to present a low winding factor. In addition, both the MMF and EMF harmonic content in single-layer windings is higher than in double-layer windings, so torque pulsations are increased as well acoustic noise emissions. To minimize the abovementioned problems the number of pole pairs p and the number of stator slots Q must be similar but not equal. This condition is attained when $Q \pm 2 = 2p$.
2. To increase the phase inductances and reduce the short circuit currents, the slots in the stator should be deep enough [25]. The phase impedance calculated as $Z_{ph} = E_{max}/I_s$ must be close to 1 p.u., i.e.

$$Z_{ph} = 2\pi f_b L_b \tag{60}$$

f_b being the base value of the electrical frequency and L_b the base value of the phase inductance, which is calculated as,

$$L_b = \psi_b / I_{s,N} \tag{61}$$

The peak base value of the flux linkage Ψ_b is,

$$\psi_b = E_{\max} / \omega_b \tag{62}$$

E_{max} being the peak value of the back-EMF, and ω_b the base electrical angular frequency, defined as $\omega_b = 2\pi f_b$. Both the air gap and slot impedances L_g and L_s in (51) and (52), respectively, are adjusted during the optimization process, in order to force the value of L_b to converge to L_{ph}. Therefore if L_b differs from L_{ph} more than a specified tolerance, the value of d_3 is changed accordingly to fulfill $L_b \approx L_{ph}$, thus starting a new iteration from (35).

V. The Multi-objective Optimization Process

Multi-objective optimization problems involve optimizing simultaneously more than one objective function, where often trade-offs between conflicting objectives must be taken. Electric motors are known to be complex and non-linear systems but in most optimal motor designs, a single-objective function is selected [27]. Typical objectives are minimum cost, highest efficiency or minimum weight. An electric machine is usually defined by a rather large number of parameters, including geometric dimensions, material characteristics, winding configurations [28] and some constrains. Therefore, to achieve an optimal design of the AFPM it seems reasonable to apply a multi-objective approach based on a genetic algorithm (GA) since GAs are mathematical methods well-suited for solving constrained and unconstrained single- or multi-objective optimization problems. These algorithms have been successfully applied in problems dealing with highly nonlinear, non-differentiable or stochastic objective functions [19] and specifically in the optimal design process of electric machines [29-31].

GAs are based on the concept of natural selection through the survival of the most suitable individuals, so that the individuals producing a least fitted solution have a small probability of reproduction whereas those producing the most fitted solutions have a greater chance [27]. The iterative heuristic search produced by the GA randomly selects a set of individuals from the current population at each step, which represents the chromosomes and after some generations the solution tends to an optimum. The specimens which produce a local optimal are the solution selected at each step and the parents of the offspring individuals for the next generation. By repeating this process, a population of individuals which evolves toward an optimal solution is produced.

Genetic algorithms perform mathematical operations to imitate genetic reproduction mechanisms including individual's selection (parents for the next generation), crossover operation (combines two parents' solutions to produce children solutions for the subsequent generation), and mutation (applies random changes to parents and children solutions) with the aim of obtaining an optimal solution.

Due to the quite large number of parameters involved in the design process of an electric machine, to limit the complexity and computational burden of the optimization process it is required to identify a reduced set of parameters which most significantly affects the performance of the analyzed machine [28]. This paper deals with ten parameters whose values are changed during the optimization process, which are shown in Table II. These parameters are coded into binary strings forming the chromosomes. The elitist scattered crossover operation is applied, which at each generation produces a random binary vector from which the genes of both parents are combined to form the offspring, as indicated in Fig. 5. Next, the mutation process is applied, by which the GA creates small random variations in each bit of the chromosomes, providing genetic diversity and enabling GA to search for wider spaces. The whole process is repeated until an established tolerance criterion is achieved; this could be either the ratio of change between consecutive solutions or the maximum number of generations which is previously settled.

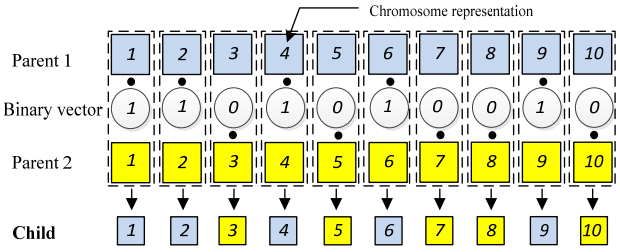

Figure 5. Scattered crossover representation when dealing with ten input variables.

VI. Model Refinement through 3D FEM Assistance

Therefore, Once the an optimal solution has been obtained by means of the optimization method based on the analytical equations explained in sections 3-5 (step 1 in Fig. 6), and in order to improve the accuracy of the final design attained, a further refinement is carried out with the help of 3D-FEM simulations of the optimized motor (step 2 in Fig. 6). However, it is well known that 3D-FEM simulations have a high computational burden, so the number of simulations must be minimized.

Therefore, a 3D-FEM model of the AFPM is generated from the solution attained in step 1. Since the air gap flux density B_g is one of the major design parameters in determining the AFPM performance, the value of B_g obtained in step 1 is compared with the one obtained by

means of the 3D-FEM model. In the case of discrepancy, a next iteration is started by adjusting the B_g value in (22) to that obtained in the FEM simulation, therefore calculating a new solution of the AFPM design. This process is iterated until the error between the B_g value obtained by means of the optimization process based on the analytical equations and the B_g value obtained through the 3D-FEM simulations is less than a specified tolerance. However, even attaining the pre-established B_g value, it does not ensure to fulfill the design specifications such as output power and torque, or power density among others, so a final validation of the obtained design is highly desirable (see Section VIII). It is worth noting that with only three iterations of this last loop, the convergence was attained.

Fig. 6 shows the design process flowchart applied in this paper.

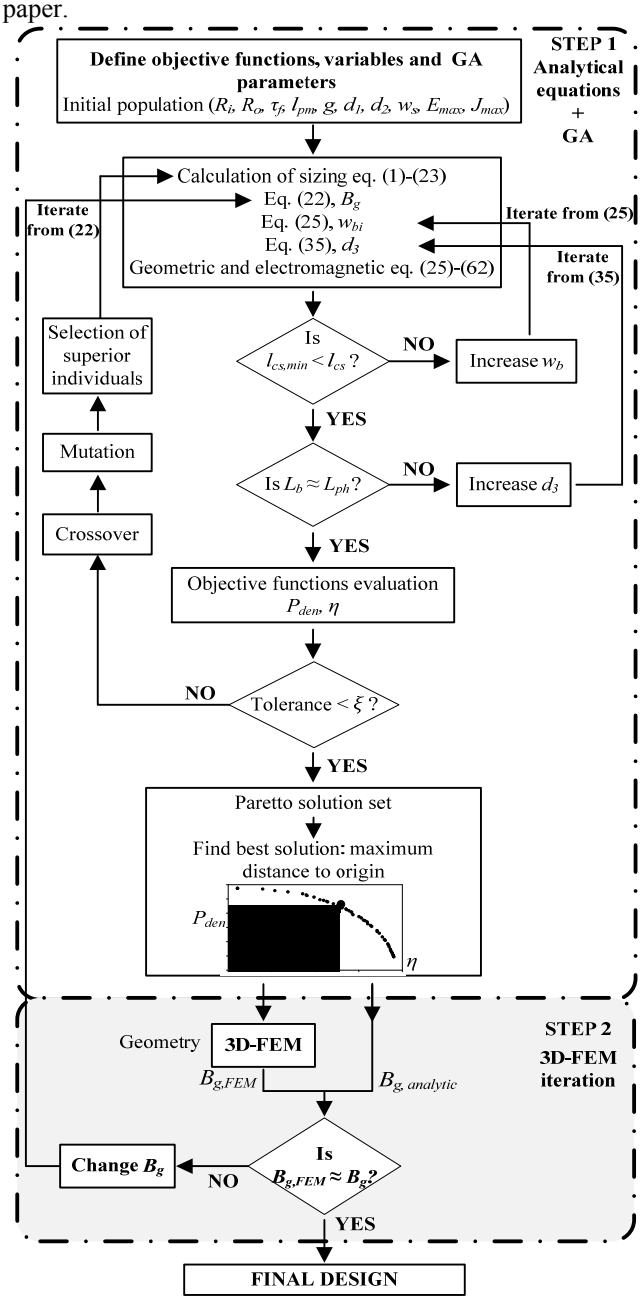

Figure 6. Design process flowchart

VII. RESULTS

This section shows the results attained by applying the MoGA with the fault-tolerance constraints.

In this paper there are some fixed parameters whose values don't change during the optimization process, which are detailed in Table I. They include the desired output power, base speed, number of phases, pole pairs, number of slots, and desired flux density in the stator and rotor cores, which greatly determine the AFPM size and performance, as well as the main properties of the materials dealt with.

TABLE I. FIXED PARAMETERS AND REQUIREMENTS OF THE FIVE-PHASE AFPM

Quantity	Symbol	Magnitude
Output power	P_{out}	2000 W
Base speed	N	1100 rpm
Output torque	T_{out}	17.36 Nm
Number of phases	m	5
Base electrical frequency	f	165 Hz
Pole pairs	p	9
Number of slots	Q	20
Laminations width	S_{lw}	0.35mm
Saturation flux density	B_{sat}	1.5 T
Slot fill factor	k_{cp}	0.5
Laminations type	*M330-35A*	-
Lamination stacking factor	k_{st}	0.95
Steel laminations mass density	ρ_{steel}	7600 kg/m3
Wire insulation thickness	W_i	0.5-2 mm
Conductors material	*Copper*	-
Conductors conductivity at 25ºC	ρ_{cu}	16.78 nΩ·m
Permanent magnets (PM) mass density	ρ_m	7400 kg/m3
PM relative permeability	μ_r	1.05
PM remanent flux density	B_r	1.3 T
Stator core flux density (peak value)	B_{sc}	1.8
Rotor core flux density (peak value)	B_{rc}	1.7

The input or design variables, that is, the variables whose values are changed during the optimization phase to explore the whole set of possible solutions, are shown in Table II. The number of design variables is usually a tradeoff between model accuracy and complexity due to the large number of possible combinations to be analyzed during the optimization process. Therefore, this paper deals with the ten most influencing design variables.

TABLE II. DESIGN VARIABLES OF THE FIVE-PHASE AFPM

Quantity	Symbol	Magnitude
Machine inner radius	$x(1)= R_i$	0.03-0.1 m
Machine outer radius	$x(2)= R_o$	0.06-0.2 m
Magnet spacer width	$x(3)= \tau_f$	1-5 mm
Magnet thickness	$x(4)= l_{pm}$	2-9 mm
Air gap length	$x(5)= g$	0.5-1.5 mm
Slot tip length	$x(6)= d_1$	1-4 mm
Slot tip shoe length	$x(7)= d_2$	1-2 mm
Slot width/opening	$x(8)= w_s$	2-10 mm
Peak value of the back-EMF	$x(8)= E_{max}$	24-60 V
Maximum conductor current density	$x(10)= J_{max}$	2-5 A/mm^2

The multi-objective optimization process considers two objective functions, i.e. the AFPM power density and efficiency. The main parameters of the MoGA include a population size of 1400 individuals, the maximum number of generations is 200, the probability of crossover is 0.8 and the probability of mutation is 0.01.

Fig. 7 shows all solutions explored by the MoGA algorithm and the Pareto front. From all this set of solutions, the one maximizing the Euclidean distance to the origin point is selected as the best solution.

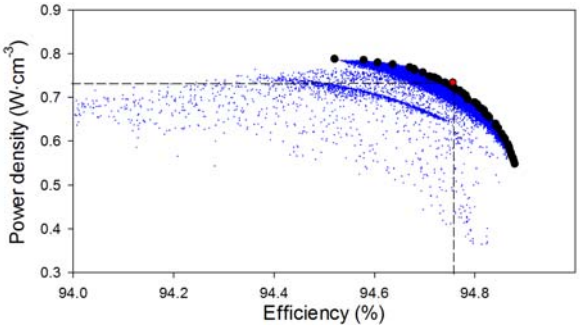

Figure 7. Analyzed solutions and Pareto front of the fitness function obtained by applying the MoGA solver.

Table III summarizes some of the main parameters of the best solution attained by means of the MoGA approach.

TABLE III. RESULTS ATTAINED BY APPLYING FAULT-TOLERANCE RESTRICTIONS

Quantity	***Symbol***	**Magnitude**
Power Density	P_{den}	72931 W/m^3
Efficiency	η	94.75%
Rotor outer radius	R_o	0.10 m
Rotor inner radius	R_i	50 mm
Number of turns per phase	N_{ph}	52
Air gap length	g	0.9 mm
Axial length of machine	l_t	87 mm
Magnet thickness	l_{pm}	4 mm
Rotor thickness	l_{cr}	15.2 mm
Stator thickness	l_{cs}	48.1 mm
Phase inductance	L_{ph}	1.1 mH
Phase resistance	R_{ph}	0.007 Ω
Air gap flux density (peak value)	B_g	0.689 T
Current per phase (peak value)	I_{ph}	18.5 A
EMF per phase (peak value)	E_{max}	21.59 V

VIII. MODEL VALIDATION THROUGH FEM

As it is well known, although radial-flux machines are often simulated by means of two-dimensional finite elements analysis, an axial flux machine must be modeled by means of three-dimensional finite elements methods (3D-FEM) due to its inherent three-dimensional geometry. Therefore, an accurate three-dimensional FEM model of the analyzed AFPM with around $1.4 \cdot 10^6$ tetrahedral volumetric elements was carefully prepared in the Flux-Cedrat® environment. This model includes all geometrical and physical characteristics of the machine components, including the electric circuit. Using this modeling system it is possible to obtain diverse type of electric and magnetic quantities of the AFPM obtained through the optimization process with very high accuracy, thus allowing to verify the excellent motor performance obtained by means of the method applied in this paper. The motor was supplied by means of five balanced voltage sources (72º phase shift between two consecutive phase voltages).

Fig. 8 plots the 3D-FEM model along with the permanent magnets and a partial view of the 3D-mesh applied in the FEM simulations.

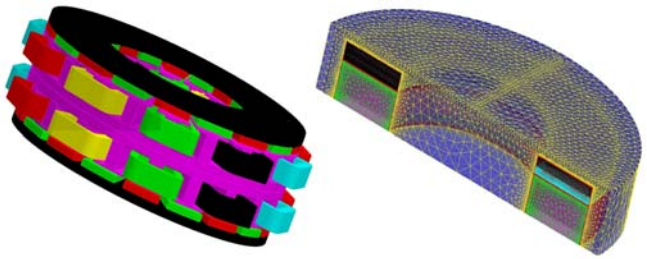

Figure 8. Three dimensional model and mesh.

Fig. 9 shows the magnetic flux distribution within the AFPM analyzed where it is proved that the flux density in the rotor laminations is almost stationary.

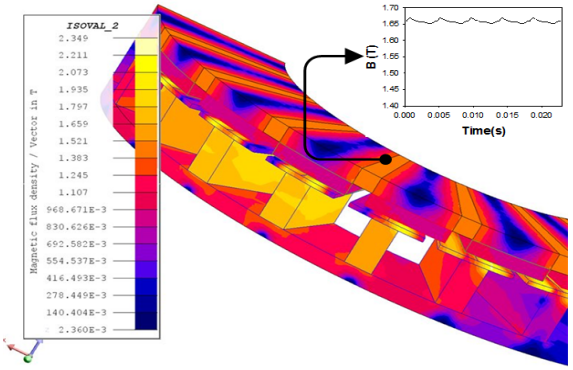

Figure 9. 3D-FEM results. Flux density distribution

Fig. 10 shows the output torque, back-EMF and phase inductance obtained through 3D-FEM simulations

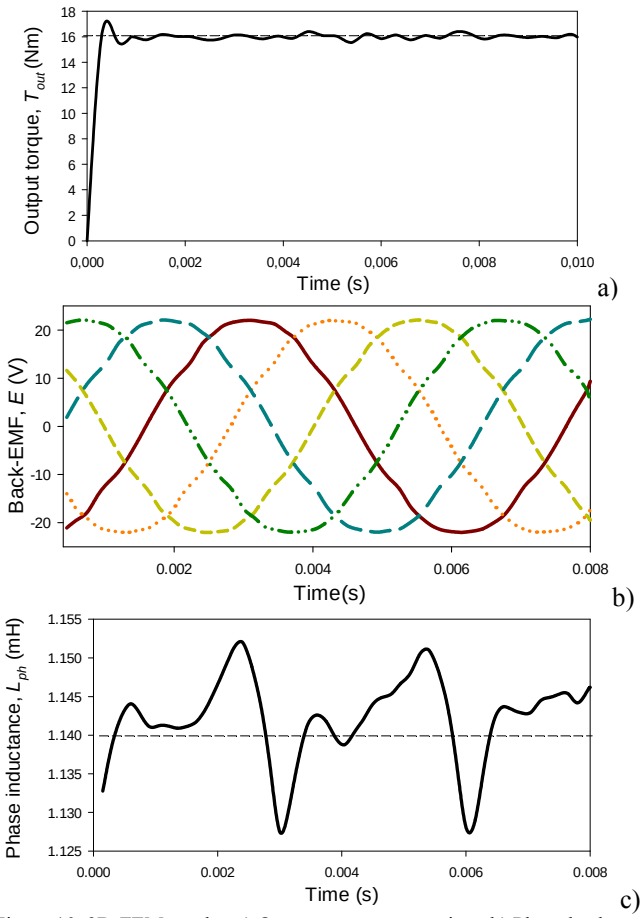

Figure 10. 3D-FEM results. a) Output torque versus time. b) Phase back-EMF. c) Phase *a* inductance.

Table IV compares some of the important parameters of the AFPM calculated by means of the design method applied in this work and by the 3D-FEM approach. These results corroborate the accuracy and usefulness of the applied optimization design method.

TABLE IV. RESULTS ATTAINED

Quantity	**Optimization method**	**3D-FEM**	**Relative error**
B_g, air gap flux density (peak value)	0.689 T	0.711T	3.19%
T_{out}, output torque	17.36 Nm	15.70 Nm	9.56%
E_{max}, back-EMF (peak value)	21.59 V	22.04 V	3.75%
L_{ph}, phase inductance	1.10 mH	1.14 mH	3.64%

IX. CONCLUSIONS

In this paper a five-phase fault-tolerant axial-flux permanent magnet synchronous motor has been designed by applying a multi-objective optimization approach based on a genetic algorithm. The design process has been assisted by means of a hybrid method combining a set of analytical equations and 3D-FEM simulations, taking care of reducing the demanding computational burden due to an intensive use of 3D-FEM simulations. Some fault-tolerance requisites have been considered during the optimization process to ensure further fault-tolerance capability. Two objective functions (the power density and efficiency of the machine) are considered in the multi-objective optimization process. The accuracy of the sizing method has been validated by means of three-dimensional finite element simulations, which show great accuracy when comparing four relevant parameters that define the machine performance. These results show the usefulness and feasibleness of the applied method to design electric motors with enhanced fault-tolerance capability.

REFERENCES

[1] X. Huang, A. Goodman, C. Gerada, Y. Fang, and Q. Lu, "Design of a five-phase brushless dc motor for a safety critical aerospace application," IEEE Trans. Ind. Electron., vol. 59, no. 9, pp. 3532-3541, Sept. 2012 doi:10.1109/TIE.2011.2172170

[2] B. Abdi, J. Milimonfared, J. Shokrollahi Moghani, A. Kashefi Kaviani, "Simplified Design and Optimization of Slotless Synchronous PM Machine for Micro-Satellite Electro-Mechanical Batteries," Advances in Electrical and Computer Engineering, vol. 9, no. 3, pp. 84-88, 2009, doi:10.4316/AECE.2009.03015:

[3] A. Pop, M. Radulescu, H. Balan,"Flux-density space-harmonics minimization for an axial-flux permanent-magnet machine," 4th International Symposium on Electrical and Electronics Engineering (ISEEE), 2013, 11-13 Oct. 2013, pp. 1-5. doi: 10.1109/ISEEE.2013.6674327:

[4] JC. Urresty, JR Riba, L Romeral, "Diagnosis of Inter-turn faults in PMSMs Operating under non-stationary conditions by applying order tracking filtering". IEEE Trans Pow Electron vol 28, pp. 507-515, 2013. doi: 10.1109/TPEL.2012.2198077.

[5] JR. Riba, A Garcia, L Romeral, "Demagnetization diagnosis in permanent magnet synchronous motors under non-stationary speed conditions". Electr Pow Syst Res vol 80, pp.1277–1285, 2010. doi:10.1016/j.epsr.2010.04.010.

[6] J Cusido, L Romeral, JA Ortega, A Garcia, JR Riba, "Wavelet and PDD as fault detection techniques". Electr Pow Syst Res vol 80, pp 915-924, 2010. doi:10.1016/j.epsr.2009.12.017.

[7] M. T. Abolhassani, H. A. Toliyat, "Fault tolerant permanent magnet motor drives for electric vehicles," IEEE International Electric Machines and Drives Conference, 2009. IEMDC '09, Miami, Florida, 3- May 2009. doi: 10.1109/IEMDC.2009.5075348.

[8] L. Parsa, H. A. Toliyat, "Sensorless direct torque control of five-phase interior permanent-magnet motor drives," IEEE Trans. Ind. Appl., vol. 43, no. 4, July/Aug. 2007. doi: 10.1109/IAS.2004.1348534.

[9] H. Saavedra, J.-R. Riba, L. Romeral, "Detection of Inter-turn faults in five-phase permanent magnet synchronous motors", Advances in Electrical and Computer Engineering, "to be published"

[10] A. Mohammadpour, S. Mishra, and L. Parsa, "Fault-Tolerant operation of multiphase permanent-magnet machines using iterative learning control," IEEE Journal of Emerging and Selected Topics in Power Electronics, vol. 2, no. 2, pp. 201-2011, June 2014 doi: 10.1109/JESTPE.2013.2295537.

[11] G. Cvetkovski, P. Lefley, L. Petkovska, S. Ahmed, "Optimal Design of a novel single phase PM BLDC motor using genetic algorithm," 15th International Power Electronics and Motion Control Conference, EPE-PEMC 2012 ECCE Europe, Novi Sad, Serbia. doi: 10.1109/EPEPEMC.2012.6397227.

[12] K. Zaplatilek, J. Leuchter, "System Optimization Using a Parallel Stochastic Approach," Advances in Electrical and Computer Engineering, vol. 13, no. 2, pp. 73-76, 2013, doi:10.4316/AECE.2013.02012.

[13] L. Liberti, Se. Kucherenko, "Comparison of deterministic and stochastic approaches to global optimization", Intern. Trans. Operation. Research, vol 12, no.3, pp. 263–285, May 2005.

[14] M. Tabassum and K. Mathew, "A Genetic Algorithm Analysis towards Optimization solutions", Intern. Journal Digit. Info. Wireless Commun, vol.4 no-1, pp. 124-142, 2014.

[15] Q.-L. Deng, F. Xiao, W.-T. Huang, "Design of new-type axial flux permanent magnet in-wheel machine," IEEE International Conference on Electrical and Control Engineering 2010, pp. 5831-5834, 2010. doi: 10.1109/iCECE.2010.1463.

[16] M. Aydin, S. Huang and T.A. Lipo, "Axial flux permanent magnet disc machines: a review", In Conf. Record of SPEEDAM, pp. 61-71, May 2004.

[17] R. Benlamine, F. Dubas, S-A. Randi, D. Lhotellier, C. Espanet, "Design by optimization of an axial-flux permanent-magnet synchronous motor using genetic algorithms," 2013 International Conference on Electrical Machines and Systems, Busan, Korea, pp. 13-17, Oct. 26-29, 2013. doi: 10.1109/ICEMS.2013.6754546.

[18] H. Saavedra, J.-R. Riba, L. Romeral, "Magnet shape influence on the performance of AFPMM with demagnetization," IEEE Industrial Electronics Society, IECON 2013, pp.973-977, 10-13 Nov. 2013. doi: 10.1109/IECON.2013.6699265

[19] A.M. EL-Refaie, T.M. Jahns, "Optimal flux weakening in surface pm machines using concentrated windings," 39th IEEE IAS Annual Meeting Industry Applications Conference, 2004. Conference Record of the 2004. pp. 1038–1047, vol.2, 3-7 Oct. 2004. doi: 10.1109/IAS.2004.1348541.

[20] D. C. Hanselman, Brushless Permanent-Magnet Motor Design,McGraw-Hill Inc. New York, pp. 151-153, 1994.

[21] J.F. Gieras, R.-J. Wang, M. J. Kamper, Axial flux permanent magnet brushless machines, Kluwer Academic Publishers, pp. 38-40, New York, 2004.

[22] 112-2004-IEEE Standard Test Procedure for Polyphase Induction Motors and Generators, 2004.

[23] S. Huang, J. Luo, F. Leonardi, T, A. Lipo, "A Comparison of power density for axial flux machines based on general purpose sizing equations", IEEE Transactions on Energy Conversion, vol. 14, no 2, pp. 185-192, June 1999. doi: 10.1109/60.766982.

[24] A.M. El-Refaie, "Fault-tolerant permanent magnet machines: a review," IET Electr. Power Appl., vol. 5, no. 1, pp. 59–74, 2011. doi: 10.1049/iet-epa.2009.0117

[25] J.A. Haylock, B.C. Mecrow, A.G. Jack, D.J. Atkinson, "Operation of fault tolerant machines with winding failures," IEEE Trans. Energy Convers., vol. 14, no. 4, pp. 1490–1495, 1999. doi: 10.1109/60.815095:

[26] P. Zheng , Y. Sui , J. Zhao , C Tong , T.A. Lipo, and A. Wang, "Investigation of a Novel Five-Phase Modular Permanent-Magnet In-Wheel Motor," IEEE Trans. Magn., vol. 47, no. 10, pp. 4084-4087, Oct. 2011. doi: 10.1109/TMAG.2011.2150207.

[27] G. V. Cvetkovski, L. B. Petkovska, "Weight Reduction of Permanent Magnet Disc Motor For Electric Vehicle Using Genetic Algorithm Optimal Design Procedure", IEEE International Conference EUROCON 2009, pp. 881-888, 18-23 May 2009, St. Petesburg. doi: 10.1109/EURCON.2009.5167738.

[28] Y. Duan, D. M. Ionel, "A Review of recent developments in electrical machine design optimization methods with a permanent-magnet synchronous motor benchmark study", IEEE Trans. Ind. Appli., vol. 49, no. 3, pp. 1268-1275, May/June 2013. doi: 10.1109/TIA.2013.2252597:

[29] T. Ishikawa, K. Nakayama, N Kurita, F.P. Dawson, "Optimization of rotor topology in pm synchronous motors by genetic algorithm considering cluster of materials and cleaning procedure", IEEE Trans Magnet, vol:50, no. 2, doi: 10.1109/TMAG.2013.2282365:

[30] S Shamlou, M Mirsalim, "Design, optimisation, analysis and experimental verification of a new line-start permanent magnet synchronous shaded-pole motor", IET Electric Power Applications, vol. 7, no. 1,pp. 16-26, 2013. doi: 10.1049/iet-epa.2012.0064.

[31] K. Hong-seok, Y Yong-Min, K Byung-il, "Rotor shape optimization of interior permanent magnet BLDC motor according to magnetization direction", IEEE Trans. Magnet, vol.. 49, no 5, pp. 219-2196, 2013. doi: 10.1109/TMAG.2013.2242056.